

# Intensity-only optical compressive imaging using a multiply scattering material : a double phase retrieval system

Boshra Rajaei<sup>1,5,6</sup>, Eric W. Tramel<sup>2</sup>, Sylvain Gigan<sup>3,6</sup>, Florent Krzakala<sup>2,6</sup>, Laurent Daudet<sup>1,4,6</sup>

<sup>1</sup>*Institut Langevin, ESPCI and CNRS UMR 7587, Paris, F-75005, France*

<sup>2</sup>*LPS-ENS, UPMC and CNRS UMR 8550, Paris, F-75005, France.*

<sup>3</sup>*Laboratoire Kastler Brossel, UPMC, ENS, Collège de France, CNRS UMR 8552, Paris, F-75005, France*

<sup>4</sup>*Paris Diderot University, Sorbonne Paris Cité, Paris, F-75013, France*

<sup>5</sup>*Sadjad University of Technology, Mashhad, Iran*

<sup>6</sup>*PSL Research University, F-75005 Paris, France*

In this paper, the problem of compressive imaging is addressed using natural randomization by means of a multiply scattering medium. To utilize the medium in this way, its corresponding transmission matrix must be estimated. To calibrate the imager, we use a digital micromirror device (DMD) as a simple, cheap, and high-resolution binary intensity modulator. We propose a phase retrieval algorithm which is well adapted to intensity-only measurements on the camera, and to the input binary intensity patterns, both to estimate the complex transmission matrix as well as image reconstruction. We demonstrate promising experimental results for the proposed algorithm using the MNIST dataset of handwritten digits as example images.

## INTRODUCTION

From the perspective of image processing, the goal of compressed sensing (CS) is to reconstruct a high-resolution sparse image, which is sparse in either the ambient domain or some transform basis, using few incoherent linear projections [1]. Over the past decade, there has been a tremendous amount of work in the field of CS, including analytical reconstruction guarantees as well as developments of new algorithmic approaches that provide efficient methods of solving the reconstruction task [2, 3]. However, to date there have only been only a handful of engineering projects where optical imagers based on CS have actually been built. Indeed, performing these incoherent (usually random) projections is a highly non-trivial step, requiring innovative hardware solutions. Amongst such imagers, one can cite, without any claim of completeness, several single-pixel imaging systems [4–6], a random lens camera [7], and an imaging setup based on a rotating diffuser [8].

The work presented in this paper is built upon a recently developed optical CS setup [9] that uses a multiply scattering medium to effect the random projection operation. The fundamental difference with this approach and most of the CS systems discussed above is that here the random projections are not designed beforehand and then implemented through sophisticated hardware, as in [10], but are based on the natural randomization properties of coherent light multiply scattering through a layer of material, in our case, Zinc Oxide. Here, the word “multiply” refers to the fact that the thickness of the material slab is many times larger than the mean free path, ensuring that the light beam is fully scattered without any remaining ballistic photons at the output. If  $x$  is the incoming wavefield (the object to be imaged in the input plane), the scattering operation is well modeled by a simple linear operator  $\mathbf{H}$ , called transmission matrix (TM).

If  $y$  is the output wavefield, discretized by receptor pixels, in the ideal noiseless case we have

$$y = \mathbf{H}x. \quad (1)$$

It has been shown that the TM of a scattering material is statistically identical to an i.i.d. random matrix with a complex Gaussian distribution [11]. The benefits of using such a system for CS imaging are that one does not have to rely on complex engineering solutions to provide the (pseudo-) randomization, and also that, in theory, only one shot is necessary to obtain any desired number of output features; as opposed to the single-pixel camera which intrinsically requires sequential measurements. There is, however, an obvious price to pay: the need of a precise calibration step. Indeed, to be able to use this system as an imaging device, i.e. to estimate  $x$  given measurements  $y$ , one has to have accurate knowledge of the matrix  $\mathbf{H}$ . This can be done accomplished by sending a series of known images, measuring the corresponding outputs, and performing a least-squares estimate on  $\mathbf{H}$ . The calibration step is conducted by shaping the input wavefront with a Spatial Light Modulator (SLM), which is only used for calibration and display, and is not part of the direct imaging system.

In this paper, we circumvent one major limitation of the previous proof-of-concept system [12]. Since optical sensors (here, a CCD camera) only measure the field intensity  $|y|^2$ , the input image was phase-modulated using a phase-only SLM, with relative phases 0,  $\pi/4$ ,  $\pi/2$ , and  $3\pi/4$ . Combining the corresponding four output intensity images, one can easily recover the complex field  $y$ —a method known as “phase-stepping holography.” Furthermore, such phase-only modulated images have a constant intensity. To obtain an image that is sparse in the spatial domain, one had to make the difference between 2 complex phase-only images which only differed by a sparse number of pixels. Therefore, in order to

get the complex measurements corresponding to a single sparse image, one had to make 8 intensity measurements. This significantly slowed down both the calibration and measurement process. Furthermore, a sufficiently fast continuous-phase SLM is a very expensive device, with limited pixel counts. The SLM used in [12] could only display  $32 \times 32$  images, for example.

Here, we investigate the alternative use of a digital micro-mirror device (DMD) as an SLM, as shown on Fig. 1. This has many advantages: DMDs are cheap, fast, and have high pixel counts. However, the main issue of using these *binary intensity* modulators is that, without additional hardware, one can no longer use phase-stepping to measure the complex output field. Instead of using some hardware to measure amplitude and phase, we resort to the so-called “phase retrieval” approach in order to estimate the missing phases from intensity-only measurements  $|y|^2$ . It should be noted that, in this framework, phase retrieval must be applied twice successively: first, for the calibration, and second, for the imaging itself. The success of the second step crucially depends on the first one, as every error on the estimation of  $\mathbf{H}$  results in multiplicative noise (also called model error) for the sparse imaging step. It should also be noted that the signal-to-noise ratio is relatively poor, thus favoring Bayesian phase retrieval techniques where noise is explicitly modeled.

The main contributions of this paper are as follows:

- A new Bayesian phase retrieval algorithm known as phase retrieval Swept AMP (prSAMP). prSAMP originates from prGAMP [13] and SwAMP [14] and is designed to work with noisy ill-conditioned transmission matrices.
- The experimental demonstration that prSAMP is efficient both for calibration of the non-sparse measurement matrix  $\mathbf{H}$  using binary inputs, and for intensity-only CS imaging of sparse inputs.

Although our previous studies [12] demonstrated a proof-of concept that CS-based imaging can be made with multiply scattering materials, we believe that this one-shot imager represents a very significant step towards real-life applications of these techniques.

## THEORETICAL MODELING

Starting from the idealized model of Eq. (1), we formalize the calibration procedure, as in [9]. The complex-valued TM,  $\mathbf{H}$ , is estimated given  $P$  known rasterized binary input images  $\mathbf{x}_p$  of size  $N = n_1 \times n_2$ , collected as columns of a matrix  $\mathbf{X}$  (of size  $N \times P$ ). Their corresponding intensity measurements,  $|y_p|$ , on  $M$  output pixels, are collected as columns of a matrix  $\mathbf{Y}$  (of size

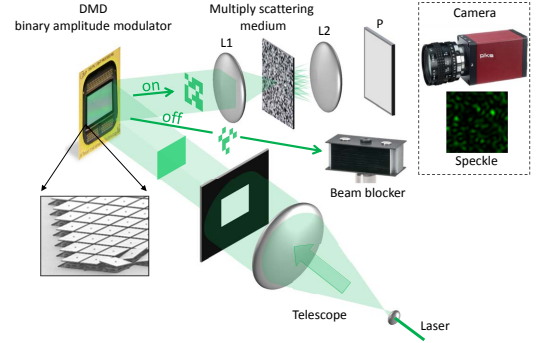


FIG. 1. Experimental setup of the imager (from [9]). A monochromatic laser at 532nm is expanded by a telescope and illuminates the SLM (here, a DMD DLP9500 from TI, with  $1920 \times 1080$  pixels). The light beam carrying the image is then focused on a random medium by means of a microscope lens. Here, the medium is a thick (several tens of microns) and opaque layer of Zinc Oxide nanoparticles, deposited on a microscope glass slide. The transmitted light is collected on the far side by a second lens, passes through a polarizer, and is detected by a standard monochrome CCD camera (AVT PIKE F-100). Note that the DMD is only here for calibration and display, and is not part of the imager itself.

$M \times P$ ). Taking the conjugate-transpose the transmission equation gives  $\mathbf{Y}^H = |\mathbf{X}^H \mathbf{H}^H|$ .

The set  $\mathbf{X}$  of calibration patterns is now seen (up to conjugate-transposition) as a new sensing matrix, and the calibration of the transmission matrix  $\mathbf{H}$  now boils down to  $M$  parallel phase retrieval problems, for each column of  $\mathbf{H}^H$  independently, with the modulus of the corresponding column  $\mathbf{Y}^H$  as a measurement,

$$\mathbf{y}_m = |\mathbf{X} \mathbf{h}_m|, \quad (2)$$

where  $\mathbf{X} \in \{0, 1\}^{P \times N}$  indicates  $P$  rasterized binary input patterns,  $\mathbf{h}_m \in \mathbb{C}^N$ ,  $m = 1 \dots M$  is the  $m$ -th row of the unknown  $M \times N$  matrix and  $\mathbf{y}_m \in \mathbb{R}_+^P$  is its corresponding measurement. The process of recovering a signal from only the magnitude of the projections is the goal of phase retrieval [13, 15, 16]. Apart from additional noise in the measurements, what makes solving Eq. (2) challenging is using binary input patterns, since most well-known phase retrieval methods work well with complex-valued measurement matrices. We have fixed this issue by mixing the ideas of Swept Approximate Message Passing (SwAMP) [14], which demonstrates good convergence properties even for ill-conditioned and noisy matrices, with the phase retrieval method prGAMP [13]. The new prSAMP algorithm is explained in the next section.

After calibration, the setup can be used as a generalized CS imager, with non-linear (intensity) measurements. In this reconstruction phase, the noiseless model turns into  $\mathbf{y} = |\mathbf{H} \mathbf{x}|$  where  $\mathbf{H} \in \mathbb{C}^{M \times N}$  is the calibrated TM and  $\mathbf{x} \in \{0, 1\}^N$  and  $\mathbf{y} \in \mathbb{R}_+^M$  are unknown sparse

binary input and its observed output intensity measurement, respectively. We use the same prSAMP method with different priors to solve the reconstruction task.

### PRSAMP ALGORITHM

In the context of CS, AMP is an iterative algorithm for the reconstruction of a sparse signal from a set of under-determined linear noisy measurements  $\mathbf{y} = \mathbf{H}\mathbf{x} + \mathbf{w}$ ,  $\mathbf{w} \sim \mathcal{N}(0, \sigma^2)$  [17]. The method originates from belief propagation, but with significantly fewer messages. It has been shown to be effective with a minimal number of measurements while being efficient in terms of computational complexity. Using a Bayesian approach [18], the main loop of AMP consists in iteratively updating the mean  $\mathbf{x}_m$  and variance  $\mathbf{x}_v$  of the unknown signal until convergence :

$$\begin{aligned} \mathbf{v}^t &= \mathbf{H}\mathbf{x}_v^{t-1}, \omega^t = \mathbf{H}\mathbf{x}_m^{t-1} - (\mathbf{y} - \omega^{t-1})\mathbf{v}^t(\mathbf{v}^t + \sigma^2)^{-1} \\ \mathbf{s}^t &= [\mathbf{H}^T(\mathbf{v}^t + \sigma^2)^{-1}]^{-1}, \mathbf{r}^t = \mathbf{s}^t\mathbf{H}^T(\mathbf{y} - \omega^t)(\mathbf{v}^t + \sigma^2)^{-1} \\ [\mathbf{x}_m^t \ \mathbf{x}_v^t] &= p_{in}(\mathbf{r}^t, \mathbf{s}^t) \end{aligned}$$

where  $p_{in}$  is a function based on the input prior. For calibration and reconstruction phases, we use Gaussian and binary priors, respectively [19, 20]. From [11], we know that the TM of a random medium appears as i.i.d. random matrices. Therefore, a Gaussian prior for calibration phase is a reasonable choice. In the reconstruction phase, two binary priors have been investigated based on provided information on the sparsity level. The details are explained in next section.

Generalized AMP (GAMP) [13] is an extension of AMP for arbitrary noise channels,  $\mathbf{y} = q(\mathbf{H}\mathbf{x} + \mathbf{w})$ , by adding an output function,  $p_{out}$ , which is dependent on the stochastic description of  $q(\cdot)$ . In normal AMP we have  $p_{out} = (\mathbf{y} - \omega^t)(\mathbf{v}^t + \sigma^2)^{-1}$  and  $p'_{out} = -(\mathbf{v}^t + \sigma^2)^{-1}$ . The convergence of both AMP and GAMP has been proved for zero-mean i.i.d. measurement matrices [21], however, they do not necessarily converge for generic matrices [22]. There have been some attempts to prevent divergence of AMP-based methods [14, 23, 24]. In [14], the authors show that a simple change in the main AMP loop may stabilize AMP significantly. They propose a sequential, or *swept*, random update of AMP backward messages, i.e.  $\mathbf{s}^t$ ,  $\mathbf{r}^t$ ,  $\mathbf{x}_m^t$  and  $\mathbf{x}_v^t$ , instead of the standard parallel calculation.

We employ a generalized version of SwAMP with a suitable phase retrieval output prior proposed in [13]

$$\begin{aligned} p_{out} &= \omega(\mathbf{v} + \sigma^2)^{-1}(r_0\mathbf{y}|\omega|^{-1} - 1) \\ p'_{out} &= (\mathbf{v} + \sigma^2)^{-1}[\mathbf{y}^2(1 - r_0^2)(\mathbf{v} + \sigma^2)^{-1} + \sigma^2\mathbf{v}^{-1}] - \mathbf{v}^{-1} \end{aligned}$$

where  $r_0 = \frac{I_1(\phi)}{I_0(\phi)}$ ,  $I_0$  and  $I_1$  are  $0^{th}$  and  $1^{st}$  order modified Bessel functions of first kind, respectively, and

---

### Algorithm 1: phase retrieval Swept AMP (prSAMP)

---

**Input** :  $\mathbf{x}_m^0, \mathbf{x}_v^0$   
**Output**:  $\mathbf{x}_m^t$   
 $\omega^0 \leftarrow 0$   
**for**  $t = 1$  **to**  $T_{max}$  **do**  
  Calculate  $\mathbf{v}^t, \omega^t, p_{out}$  and  $p'_{out}$ .  
   $rp \leftarrow \text{Random-Permutation}([1 \dots N])$   
  **foreach**  $i$  **in**  $rp$  **do**  
    Calculate  $s_i^t, r_i^t, x_{mi}^t$  and  $x_{vi}^t$   
     $\mathbf{v}_{old} \leftarrow \mathbf{v}^t, \omega_{old} \leftarrow \omega^t$   
     $\mathbf{v}^t \leftarrow \mathbf{v}_{old} + \mathbf{h}_i(x_{vi}^t - x_{vi}^{t-1})$   
     $\omega^t \leftarrow \omega_{old} + \mathbf{h}_i^2(x_i^t - x_i^{t-1}) - p_{out}(\mathbf{v}^t - \mathbf{v}_{old})$   
    Calculate  $p_{out}, p'_{out}$   
  **Until** Convergence

---



FIG. 2. Instance structured patterns used in calibration phase.

$\phi = 2\mathbf{y}|\omega|(\mathbf{v} + \sigma^2)^{-1}$ . The algorithm is called prSAMP and is described in Algorithm 1.

### EXPERIMENTAL RESULTS

To investigate the performance of the imaging system, two binary datasets were constructed from the spatially-sparse MNIST handwritten dataset. The first,  $D_1$ , consists of cropped digit images at a resolution of  $20 \times 20$  pixels ( $N = 400$ ). The second,  $D_2$ , was constructed by rescaling the MNIST dataset to  $32 \times 32$  pixels ( $N = 1024$ ). Both  $D_1$  and  $D_2$  retain the original MNIST training/testing partition.

For the calibration step, the training set of  $D_1$  was modified by randomly exchanging  $5 \times 5$  blocks of pixels between digit images. Fig.2 shows a few samples of these structured patterns. This structured randomization was done to reduce the effect of correlation between the DMD pixels. Additionally, to avoid the possibility of one completely zero, or very sparse, lines in  $\mathbf{X}$  (see Eq. (2)), we introduce a fixed number of unstructured i.i.d. Bernoulli random binary patterns to the calibration training set.

The TM is then calculated using  $P = \lceil \alpha N \rceil$  calibration images for the oversampling ratio  $\alpha > 1$ , of which the first  $N$  are Bernoulli random patterns. At the receptor,  $M$  samples are randomly selected from a  $100 \times 100$  region of the output image.

Fig. 3 shows the performance of the proposed calibration method for varying values of  $\alpha$ . In lieu of ground-truth comparisons for TM estimation, we assess the calibration performance in terms of “depen-

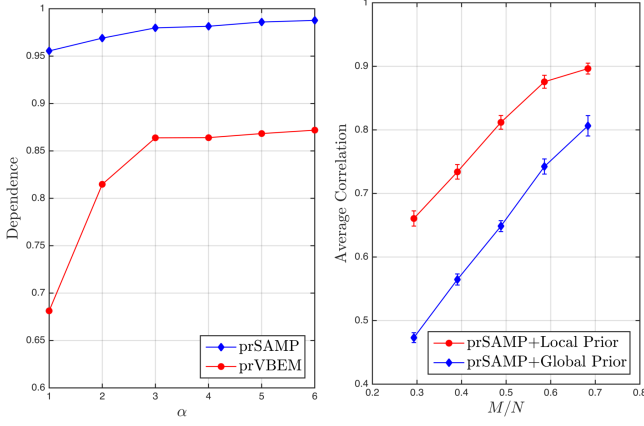


FIG. 3. **Left:** Calibration performance of both prSAMP and prVBEM for varying numbers of displayed patterns  $P = \lceil \alpha N \rceil$  which are generated from the  $D_1$  dataset. **Right:** Reconstruction performance over 50 digits of  $D_2$  ( $N = 1024$ ) using prSAMP with both global and local binary priors for  $M = \{300, 400, 500, 600, 700\}$  output samples.



FIG. 4. Visual performance of prSAMP algorithm over  $32 \times 32$  images. First row shows the original images, second and third rows show reconstructions from prSAMP using local and global binary priors, respectively, for  $M = 700$ .

dence,” the normalized cross-correlation, sans mean removal,  $\left\langle \frac{\mathbf{y}}{\|\mathbf{y}\|}, \frac{|\mathbf{H}\mathbf{x}|}{\|\mathbf{H}\mathbf{x}\|} \right\rangle$ , between observed samples and the predicted output of known input patterns using the estimated TM. We measure dependence over 400 digits from the testing set of  $D_1$ . We compare the level of achieved dependence between prSAMP and prVBEM [9], a “mean-field” variational Bayes phase retrieval technique we previously employed for the task of TM calibration in the context of light focusing.

After calibration, the direct imaging phase can start. As we explained in Section , calibration and reconstruction steps are performed using the same prSAMP algorithm, but with a different input prior. During calibration, we assume a complex Gaussian prior since the TM is modeled as i.i.d. random. However, for reconstruction, a binary prior is required,

$$x_{mi}^t = z^{-1} \rho_i e^{\frac{-|1-r_i^t|^2}{2s_i^t}}, \quad x_{vi}^t = x_{mi}^t - (x_{mi}^t)^2, \quad (3)$$

$$\text{where } z = (1 - \rho_i) e^{\frac{-|r_i^t|^2}{2s_i^t}} + \rho_i e^{\frac{-|1-r_i^t|^2}{2s_i^t}},$$

where  $\rho_i$  indicates the probability of pixel  $i$  to be non-zero. We use two strategies to set this parameter. The

first is a *global* approach which sets all  $\rho_i$  uniformly to the input image sparsity level, which we assume is known up to some tolerance. In the second *local* approach, we calculate the per-pixel non-zero probability using the calibration training set, which is a fast off-line process.

As the prior calculation must be repeated at each pixel for each sweep of the prSAMP algorithm, we select the simplest possible prior for the sake of computational efficiency. The interested reader may refer to [25] for a more sophisticated method of using learned priors for reconstruction tasks.

We next use the  $D_2$  dataset to study the effectiveness of prSAMP post-calibration reconstruction. We first perform the calibration step to estimate  $M = N$  rows of the TM using  $\alpha = 5$ , yielding an average calibration correlation of 97% over 1024 test digits. For reconstruction, we randomly choose 50 images from the test set, with five images from each digit.

The correlation of prSAMP reconstructions to the true inputs, using global and local binary priors, are compared in Fig. 3 as a function of the measurement rate  $M/N$ . Leveraging the extra information in the local prior provides an average 14.87% increase in reconstruction performance over the global prior. To visually assess the quality of recovered images, Fig. 4 provides one instance from each digit recovered at  $M = 700$ , with reconstructions using the local and the global priors. As expected, the local prior provides better subjective quality, with less spurious isolated pixels.

## CONCLUSION

In this study, a phase retrieval compressive imager has been proposed and experimentally evaluated using a simple optical setup. The imager has the potential of providing high resolution images in one shot. We solve the challenging problem of estimating a complex transmission matrix by displaying known binary patterns and solving the phase retrieval problem via swept AMP. Finally, we show that we can estimate the transmission matrix accurately, allowing it to be used for compressed sensing. Further studies are necessary to provide faster calibration methods.

## ACKNOWLEDGMENT

The authors would like to thank Christophe Schülke for his enlightening comments. This research has received funding from the European Research Council under the EUs 7th Framework Programme (FP/2007- 2013/ERC Grant Agreement 307087-SPARCS and 278025- COMEDIA) ; and from LABEX WIFI under references ANR-10-LABX-24 and ANR-10-IDEX-0001-02-PSL\*.

- 
- [1] J. Romberg, IEEE Signal Process. Mag. **25**, 14 (2008).
  - [2] Y. Eldar and G. Kutyniok, *Compressed sensing: theory and applications* (Cambridge Uni. Press, 2012).
  - [3] H. Boche, R. Calderbank, G. Kutyniok, and J. Vybíral, *Compressed Sensing and its Applications* (Springer, 2015).
  - [4] M. Duarte, M. Davenport, D. Takhar, J. Laska, T. Sun, K. Kelly, and R. Baraniuk, IEEE Signal Process. Mag. **25**, 83 (2008).
  - [5] F. Magalhães, F. Araújo, M. Correia, M. Abolbashari, and F. Farahi, Appl. Opt. **50**, 405 (2011).
  - [6] D. Shrekenhamer, C. Watts, and W. Padilla, Opt. express **21**, 12507 (2013).
  - [7] R. Fergus, A. Torralba, and W. Freeman, MIT CSAIL Tech. Report (2006).
  - [8] C. Zhao, W. Gong, M. Chen, E. Li, H. Wang, W. Xu, and S. Han, Appl. Phys. Lett. **101**, 141123 (2012).
  - [9] A. Drémeau, A. Liutkus, D. Martina, O. Katz, C. Schülke, F. Krzakala, S. Gigan, and L. Daudet, Opt. Express **23**, 11898 (2015).
  - [10] L. Gao, J. Liang, C. Li, and L. Wang, Nature **516** (2014).
  - [11] S. Popoff, G. Lerosey, R. Carminati, M. Fink, A. Boccaro, and S. Gigan, Phys. Rev. Lett **104**, 100601 (2010).
  - [12] A. Liutkus, D. Martina, S. Popoff, G. Chardon, O. Katz, G. Lerosey, S. Gigan, L. Daudet, and I. Carron, Sci. Rep. **4** (2014).
  - [13] P. Schniter and S. Rangan, IEEE T. Sigal Proces **63**, 1043 (2015).
  - [14] A. Manoel, F. Krzakala, E. Tramel, and L. Zdeborová, in *Proc. 32nd Int. Conf. Machine Learning (ICML-15)* (2014).
  - [15] E. Candes, Y. Eldar, T. Strohmer, and V. Voroninski, SIAM Rev. **57**, 225 (2015).
  - [16] M. Iwen, A. Viswanathan, and Y. Wang, arXiv preprint:1501.02377 (2015).
  - [17] A. Maleki, *Approximate message passing algorithms for compressed sensing*, Ph.D. thesis, Stanford uni. (2010).
  - [18] F. Krzakala, M. Mézard, F. Sausset, Y. Sun, and L. Zdeborová, Phys. Rev. X **2** (2011).
  - [19] F. Krzakala, M. Mézard, F. Sausset, Y. Sun, and L. Zdeborová, J. Stat. Mech: Theory Exp. **2012**, P08009 (2012).
  - [20] J. Barbier, F. Krzakala, M. Mézard, and L. Zdeborová, in *Allerton conference* (2012) pp. 800–807.
  - [21] M. Bayati and A. Montanari, IEEE Trans. Inf. Theory **57**, 764 (2011).
  - [22] F. Caltagirone, L. Zdeborová, and F. Krzakala, in *IEEE Int. Sym. Inf. Theory (ISIT)* (2014) pp. 1812–1816.
  - [23] J. Vila, P. Schniter, S. Rangan, F. Krzakala, and L. Zdeborová, in *Int. Conf. Acoustics Speech Signal Process. (ICASSP)* (2015) pp. 2021–2025.
  - [24] B. Cakmak, O. Winther, and B. Fleury, in *IEEE Inf. Theory Work.* (2014) pp. 192–196.
  - [25] E. Tramel, A. Drémeau, and F. Krzakala, arXiv preprint:1502.06470 (2015).